not been observed, are $\epsilon$ and $\zeta$ in the third band and $\rho$ in the fourth. The periods expected from these cross sections are of the order of magnitude of $P_6$, the $\delta$ cross section. A weak beating in $P_6$ has been observed and therefore may have been indicative of the presence of such periods. However, positive identification could not be made because of the distortion caused by $P_3$, which occurs with an amplitude much larger than that of $P_6$. With higher fields and higher specimen purity these cross sections should be determinable.

---

# Band Structure and Fermi Surface of Zinc

WALTER A. HARRISON
*General Electric Research Laboratory, Schenectady, New York*
(Received November 27, 1961)

The band structure of zinc is calculated using a modified orthogonalized-plane-wave method and the Hartree-Fock calculations of neutral zinc by Piper. The band structure is obtained in a form which allows it to be extended readily to slight distortions of the lattice. The calculated structure is compared to an experimental band structure obtained by adjusting the matrix elements to fit de Haas-van Alphen observations of the zinc Fermi surface. The band energies do not differ by more than 0.04 ry for the two treatments. The Fermi surface from the experimental band structure is drawn in some detail. One matrix element is found to be only 0.004 ry, requiring an analysis of magnetic breakdown in the interpretation of experiments. The probability of band-to-band transitions, calculated explicitly in the high-field limit, is continued into the low-field range with a result equivalent to Blount's low-field result. The formulas for the intermediate range are applied to zinc.

## I. INTRODUCTION

THE motivation for undertaking a detailed band-structure determination is based on several major changes in the nature of our understanding of the electronic structure of metals:

(a) Extensive experimental work[1] has established in some detail and with some precision the size and shape of the Fermi surfaces in several metals.

(b) Band-structure calculations[2-6] have in several cases given a very good account of the Fermi surfaces determined experimentally.

(c) New techniques[3,7,8] make it possible to obtain the essentials of the band structure without recourse to the large amounts of effort and expense previously necessary.

(d) The discovery[1] that many of the polyvalent metals

have band structures which do not deviate greatly from a free-electron or one-OPW (orthogonalized-plane-wave) approximation gives hope that simplified approaches may allow one to treat the modifications in band structure which occur due to lattice distortions and alloying.

In this framework, it appeared appropriate to explore the influence of the band structure on various metallic properties. It was first desirable to establish with some certainty the band structure of an individual polyvalent metal; both from a full band calculation and from experimental studies of the Fermi surface. If reasonable agreement between the two were obtained, one might have some confidence in the structure, and proceed to study the influence of this structure on various properties of the metal.

In selecting a metal, it was decided that the extra richness in properties for a hexagonal metal favored it over a cubic metal. Of the hexagonal metals, zinc has been most thoroughly studied experimentally and its $c/a$ ratio deviates appreciably from that for close packing, a fact which would be interesting to explore. Furthermore, it was necessary to start from scratch in order to obtain the flexibility which would make it possible to examine changes in band structure under modifications of the lattice. Since a band structure calculation has

[1] *The Fermi Surface*, edited by W. A. Harrison and M. B. Webb (John Wiley & Sons, Inc., New York, 1960).

[2] V. Heine, Proc. Roy. Soc. (London) A240, 340, 361 (1957), aluminum.

[3] W. A. Harrison, Phys. Rev. 118, 1182 (1960), aluminum.

[4] B. Segall, Phys. Rev. Letters 7, 154 (1961), copper; Phys. Rev. 125, 1797 (1961), aluminum; (to be published), silver and gold.

[5] G. A. Burdick, Phys. Rev. Letters 7, 156 (1961), copper.

[6] L. Falicov (to be published), magnesium.

[7] J. C. Phillips and L. Kleinman, Phys. Rev. 116, 287, 880 (1959).

[8] M. H. Cohen and V. Heine, Phys. Rev. 122, 1821 (1961).

some interest of itself, it was preferable to select a metal for which no band-structure calculation had been done; this again favored zinc over magnesium. Finally, the existence of band-structure determinations in both zinc and magnesium would allow a study of the differences in their properties.

It is not possible to obtain the band structure of zinc from experimental studies of the Fermi surface alone. The band gaps associated with three lattice wave numbers[9] must be determined, and the areas of more than three segments of Fermi surface which depend on them have been measured. Unfortunately, these measurements do not uniquely determine the band gaps since the sign of the gaps (the ordering of odd and even states) is not known, and eight choices of signs are possible. Thus, eight distinct band structures could explain the same data. Furthermore, there remain some ambiguities in the interpretation, as will be seen. It is therefore necessary to perform a band calculation with at least sufficient accuracy to assign the ordering of states; then an experimental band structure can be selected which has this same ordering.

It was found that a band-structure calculation based on recent approximational techniques could be done in such a way as to allow the determination of the variation of the band gaps under distortion without appreciable extra calculation.

## II. THEORY OF THE METHOD

We wish to find the band gaps associated with each Bragg reflection plane which intersects the Fermi surface. It will then be possible, using established methods,[3] to find that portion of the band structure which is of interest. To find these gaps we use a modification of the scheme proposed by Cohen and Heine,[8] which we will describe.

The Hamiltonian for the electrons in the crystal contains the kinetic energy operator $T$ and a potential $V_{op}$ which must also be written as an operator since it is to contain exchange. The exact energy eigenstates of this Hamiltonian, $\psi_k$, are written, following Phillips and Kleinman,[7] in two terms.

$$\psi_k = \varphi_k - \sum_\alpha (\psi_\alpha, \varphi_k) \psi_\alpha. \qquad (1)$$

It is hoped that $\varphi_k$ can be made smooth. The final term guarantees the orthogonality of the conduction band states $\psi_k$ to the core states $\psi_\alpha$. Inserting this form for $\psi_k$ in the Schrödinger equation, we obtain

$$T\varphi_k + (V_{op} + V_R)\varphi_k = E_k \varphi_k, \qquad (2)$$

where

$$V_R \varphi_k = -\sum_\alpha (E_\alpha - E_k)(\psi_\alpha, \varphi_k)\psi_\alpha. \qquad (3)$$

$V_R$ is an operator which would correspond to the repulsive term in a pseudopotential approach. We could

---

[9] By a lattice wave number we mean $2\pi$ times a reciprocal lattice vector; that is, it is the change in wave number which an electron makes in a Bragg reflection.

at this point treat $V_{op} + V_R$ as small; the zero-order $\varphi_k$ become simply plane waves and the correction terms can be treated to any desired order. This would be the orthogonalized-plane-wave method.

Cohen and Heine,[8] however, have shown that we can further reduce the effective size of $V_{op} + V_R$. They note that the addition of any linear combination of core states to $\varphi_k$ does not change the wave function $\psi_k$ since such a modification is automatically subtracted out by the orthogonalization terms in Eq. (1). Therefore, one may add whatever linear combination optimizes the smoothness of $\varphi_k$. They therefore minimize the volume integral $\int |\nabla \varphi_k|^2 d\tau / (\varphi_k, \varphi_k)$ by variation of $\varphi_k$ in this manner and substitute the result in Eq. (2). This new $\varphi_k$ now satisfies Eq. (2) with

$$(V_{op} + V_R)\varphi_k = V_{op}\varphi_k - \sum_\alpha (\psi_\alpha, V_{op}\varphi_k)\psi_\alpha$$
$$+ \frac{(\varphi_k, (V_{op} + V_R)\varphi_k)}{(\varphi_k, \varphi_k)} \sum_\alpha (\psi_\alpha, \varphi_k)\psi_\alpha. \qquad (4)$$

At this point we depart from the Cohen-Heine scheme. We take the inner product of $\varphi_k$ and Eq. (4) and solve for $(\varphi_k, (V_{op} + V_R)\varphi_k)$. Substituting this back in Eq. (4), we obtain

$$(V_{op} + V_R)\varphi_k = U_{op}\varphi_k$$
$$+ \frac{(\varphi_k, U_{op}\varphi_k)\sum_\alpha (\psi_\alpha, \varphi_k)\psi_\alpha}{(\varphi_k, \varphi_k) - \sum_\alpha (\varphi_k, \psi_\alpha)(\psi_\alpha, \varphi_k)}, \qquad (5)$$

with

$$U_{op}\varphi_k = V_{op}\varphi_k - \sum_\alpha (\psi_\alpha, V_{op}\varphi_k)\psi_\alpha. \qquad (6)$$

The formal manipulations, to this point, have not involved approximations. We will now regard this final $V_{op} + V_R$ as small. Then according to Eq. (2), the zero-order $\varphi_k$ are plane waves and the matrix elements will be given by

$$(\varphi_{k+K}, (V_{op} + V_R)\varphi_k) = (\varphi_{k+K}, U_{op}\varphi_k)$$
$$+ \frac{(\varphi_k, U_{op}\varphi_k)\sum_\alpha (\psi_\alpha, \varphi_k)(\varphi_{k+K}, \psi_\alpha)}{1 - \sum_\alpha (\varphi_k, \psi_\alpha)(\psi_\alpha, \varphi_k)}. \qquad (7)$$

We may note that the band gaps are independent of the zero of energy as they should be; this was not true of the perturbation treatment of the final term in Eq. (4) suggested by Cohen and Heine.

It should also be remarked that the difference between this approach and an unmodified OPW approach is significant. The few-OPW approach using Eqs. (2) and (3) and the Hartree-Fock term values for zinc leads to significantly different results from those we will obtain.

The matrix elements associated with a Brillouin-zone face (a Bragg reflection plane) vary somewhat over that face since the potential is an operator. We may hope that variation will be small since to the extent that we could represent the crystal potential as the sum

of spherically symmetric pseudopotentials there would be no variation. Ham[10] has noted variations of a few hundredths of a rydberg in the alkali metals, and similar variations are seen in aluminum and magnesium. We will wish to use a single matrix element for each plane in determining the Fermi surface and subsequently in analyzing other properties of the crystal. In view of the uncertainty about this variation, it is desirable to evaluate the matrix elements where they are most important; that is, at the intersection of the Brillouin-zone face in question and the Fermi surface. This introduces a complication in that the matrix elements are between states of wave number $\mathbf{k}$ and $\mathbf{k}+\mathbf{K}$ which are not collinear. This minor algebraic complication, however, leads to a major reduction in the numerical work required and allows us to obtain a simple analytic expression for the matrix element as a function of lattice wave number as we shall see.

We consider the gap across the Brillouin-zone plane associated with a single lattice wave number, $\mathbf{K}$. The matrix element of $V_{op}+V_R$ between the state $\mathbf{k}$ and $\mathbf{k}+\mathbf{K}$ shown in Fig. 1 is equal to half the bandgap at $a$. The magnitude of both $\mathbf{k}$ and $\mathbf{k}+\mathbf{K}$ is equal to the free-electron Fermi wave number $k_F$.

We take the core states $\psi_\alpha$ in Eq. (7) to be simply the atomic core functions centered about each atom in the crystal; that is, we assume that the core bands are infinitely narrow. This is probably a good approximation even for the $3d$ band since the overlap between adjacent atomic orbitals is not large. Furthermore, the $3d$ band is found to lie quite low, near the minimum in the conduction band. Furthermore, we assume that $V_{op}+V_R$ may be written as a sum over all atoms of localized operators and that their overlap in adjacent cells may be neglected. This will require some care when we select the potential. It is appropriate in the evaluation of the various inner products indicated in Eq. (7) to expand the plane waves in spherical Bessel functions and spherical harmonics. Here we see the difficulty which arises since $\mathbf{k}$ and $\mathbf{k}+\mathbf{K}$ are not collinear; there is no single set of axes for which all the expansions are simple in form. It turns out to be convenient to make all of the expansions in spherical harmonics using the $z$ axis of Fig. 1 as the axis of the spherical harmonics. We write the core states in the customary fashion,

$$\psi_\alpha = r^{-1} P_{nl}(|\mathbf{r}-\mathbf{R}_\alpha|) Y_l{}^m(\theta,\varphi). \qquad (8)$$

The index $\alpha$ is used to designate the quantum numbers, $n$, $l$, and $m$ and the position $\mathbf{R}_\alpha$ of the core in question, which also serves as the center for the spherical-harmonic expansion. The plane waves are normalized to the volume of the crystal $\Omega$, and we proceed to evaluate the inner products appearing in Eq. (7). The angular integrations may all be performed, and after some labor
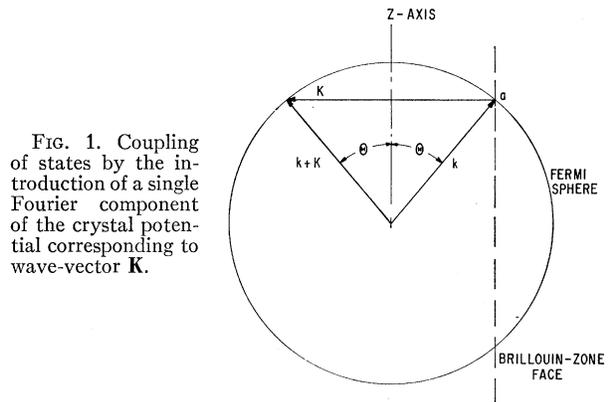
[10] F. S. Ham, reference 1, p. 23.



FIG. 1. Coupling of states by the introduction of a single Fourier component of the crystal potential corresponding to wave-vector $\mathbf{K}$.

we find the first term in Eq. (7),

$$(\varphi_{k+K}, U_{op}\varphi_k) = \left[\frac{4\pi}{\Omega}\sum_\alpha e^{-i\mathbf{K}\cdot\mathbf{R}_\alpha}\right]\sum_l (2l+1)P_l(\cos 2\Theta)$$

$$\times \left\{ \int r^2 j_l(kr) V_{op} j_l(kr) dr \right.$$

$$\left. -\sum_{n=1}^{3} \int r P_{nl}(r) V_{op} j_l(kr) dr \int x j_l(kx) P_{nl}(x) dx \right\}. \qquad (9)$$

The $P_l(\cos 2\Theta)$ are Legendre polynomials.

$$\Theta = \sin^{-1}(K/2k_F).$$

The $(\varphi_k, U_{op}\varphi_k)$ appearing in the final term of Eq. (7) may be evaluated from Eq. (9) by taking $\mathbf{K}=0$. The sums appearing in the final term of Eq. (7) are of the same form as the final sum of Eq. (9) and are obtained simply by replacing $V_{op}$ by unity in that expression.

We see here the mathematical simplification which has been effected. All integrals over the core functions and over $V_{op}$ involve only the single wave number, the free-electron Fermi wave number. Thus, the expression within the curly brackets becomes simply a set of $l$-dependent coefficients which we evaluate by a single set of integrations. This, then, leaves us with an analytic expression for all lattice wave numbers with magnitude less than $2k_F$. Thus, we may calculate the changes in the gaps arising from the motion of the Bragg planes under a distortion of the crystal. In detail it will be convenient to treat the first integral in Eq. (9) on slightly different footing as we will see when we discuss the potential.

### III. THE POTENTIAL

The potential which we will use is based on the Hartree-Fock field for neutral zinc, as determined by Piper.[11] The Hartree-Fock radial equation may be

[11] W. W. Piper, Phys. Rev. 123, 1281 (1961). This paper does not include neutral zinc, but the calculations have subsequently been extended to that case.

written in our notation:

$$\left[\frac{d^2}{dr^2}-\frac{l_\alpha(l_\alpha+1)}{r^2}\right]P_\alpha(r)-V_{op}P_\alpha(r)=\sum_\nu \epsilon_{\alpha\nu}P_\nu(r).$$

$V_{op}$ now contains several terms which we must distinguish:

(a) The self-consistent field due to the nucleus and to each of the electrons present. We include only the core electrons in this term, leaving an unscreened core potential. The screening is to be dealt with separately.

(b) Terms involving exchange between the conduction and core electrons, which are to be included in the calculation.

(c) Exchange between conduction electrons. This term has been dropped in the calculation. The author is indebted to J. C. Phillips for suggesting that it is better not to include unscreened exchange than to include it and that the errors involved in this term are probably small in polyvalent metals.

(d) Screening of the core by the conduction electrons. Two schemes were used for treating this contribution; the results will be given for each. One is expected to overestimate screening; the other to underestimate it.

(i) A Wigner-Seitz treatment of electron interactions in which the core potential is left unscreened but cut off in the region of the cell boundary.

(ii) A free-electron self-consistent screening of the net core charge, with the remainder of $V_{op}$ unscreened.

The motivation for the first approach is, of course, that a correlation hole surrounds the electron under consideration, leaving the core potential unscreened. In a divalent metal the correlation hole is presumably of the size of the volume per conduction electron, which is only half the volume of the atomic cell, so we would appear to omit more screening than we should. However, we propose to cut this Coulomb potential off at the inscribed sphere in muffin-tin fashion so this error may not be so serious. Furthermore, the conduction electrons are to quite an extent excluded from the core region by their orthogonalization to the core states which will also reduce the true screening. We conclude

that this approximation may well be preferable to free-electron screening.

In suggesting the second approach, we recognize that the screening is probably most important in connection with the Coulomb field of the net core charge since this is a long-range field. Screening would be less effective for the more localized terms in the core potential. Thus, we include only the screening where it is most important. A screened Coulomb potential was obtained by making a Fourier transform of the potential, dividing by the wave-number-dependent Hartree dielectric constant for free electrons and transforming back to obtain the screened potential. This is hoped to result in a reasonably good approximation to a full self-consistent calculation.

In both cases it was necessary to make some sort of cutoff in the neighborhood of the cell boundary since in both cases the net core potential seriously overlapped neighboring cells. In case (i), it is the $1/r$ potential which overlaps; in case (ii) it is the oscillatory $1/r^3$ term[12] in the potential. The potential was in both cases cut off at the sphere inscribed in the atomic cell and taken constant in the remainder of the cell.[13] The constant value was taken equal to the average of the potential (before cutting off) in the region between the inscribed sphere and a sphere of volume equal to the cell volume. The results were found not to be very sensitive to the exact choice of this average value.

## IV. CALCULATIONS AND RESULTS

The major calculation required was the evaluation of the integrals appearing in Eq. (9). The plane waves were expanded in terms of the form of Eq. (8), writing $n=4$. The radial $4l$ functions have the form

$$P_{4l}=rj_l(k_Fr).$$

$V_{op}$ is as described above. In integrals involving core functions it was unnessary to truncate the potential since the core functions became quite small by the time the inscribed sphere was reached. In integrals involving the potential and Bessel functions only, the Coulomb field of the net core charge was subtracted off and treated separately. The matrix elements for the residual

TABLE I. Matrix elements for the unscreened potential.

| Lattice wave number[a] | $K$ (a.u.) | $(\varphi_{k+K}, V\varphi_k)/S$[b] (ry) | $(\varphi_{k+K}, (V_{op}+V_R)\varphi_k)/S$[c] (ry) | $S=[1+\exp(i\mathbf{K}\cdot\delta)]/2$ Mag. | Phase |
|---|---|---|---|---|---|
| [002] | 1.3740 | −0.3074 | −0.0227 | 1 | 0° |
| [100] | 1.4475 | −0.2849 | −0.0042 | 1/2 | −60° |
| [101] | 1.6022 | −0.2406 | +0.0372 | √3/2 | +30° |
| [000] | 0.0000 | −2.0869 | −1.6907 | 1 | 0° |

[a] See reference 19 for notation.
[b] $V$ is the net ionic potential, $-2e^2/r$.
[c] $(\varphi_{k+K}, (V_{op}+V_R)\varphi_k)$ is the final matrix element.

[12] For a discussion of this term see, for example, W. Kohn and S. H. Vosko, Phys. Rev. **119**, 912 (1960).
[13] Such truncating schemes are discussed in detail by F. S. Ham and B. Segall, Phys. Rev. **124**, 1786 (1961).

short-range potential were calculated using $l$ values through 2.

The integrals over the potential and the orthogonality coefficients $(4\pi\int P_{4l}P_{nl}dr)$ were obtained by tabulating the $P_{4l}$ and reading them into an IBM 650 computer; Piper's Hartree-Fock program[11] then calculated the orthogonality coefficients and tables of $V_{op}P_{4l}$.[14] Integrations of the form $\int P_{nl}V_{op}P_{4l}dr$ were then calculated by hand.

The terms in $\int P_{4l}V_{op}P_{4l}dr$ arising from the Coulomb field of the net core charge [in case (i)] and the screened field [in case (ii)] were obtained by summing over all $l$ to obtain again the form of a simple Fourier transform. The integral of the truncated potential over the atomic cell was then obtained by hand for the lattice wave number of interest.

The low-temperature lattice parameters of $c=9.1453$ and $a=5.0120$ atomic units (a.u.) were obtained[15] from the room temperature values and the measured thermal expansion coefficients. The free-electron Fermi wave number is $k_F=0.8412$. The Bragg-reflection planes associated with three lattice wave numbers were found to intersect the free-electron Fermi surface. The matrix element associated with each of these was calculated; the results are given in Tables I and II. The structure factor, $S=[1+\exp(i\mathbf{K}\cdot\boldsymbol{\delta})]/2$, where $\boldsymbol{\delta}$ is the vector distance between the two atoms in the cell, was tabulated separately since its inclusion tends to obscure the variation in matrix elements arising from the details of the ionic potential. The matrix elements of the unscreened or screened net ionic Coulomb potential between plane waves are also included to indicate the extent of the cancellation which has taken place in the final results. The differences between the results for the two methods are small (a few hundredths of a rydberg), but as we will see they are important.

In the unscreened case a value is also given for the $\mathbf{K}=0$ matrix element which gives a crude estimate of the energy of the band minimum. The same value should be applicable for the screened cases since screening does not change the average value of the potential. It should be noted that the $\mathbf{K}=0$ value is not equal to the limit of the $\mathbf{K}\neq0$ matrix elements as $\mathbf{K}\to0$ since the former alone is affected by a constant term in the Hamiltonian.

TABLE II. Matrix elements for a screened potential.

| Lattice wave number[a] | $(\varphi_{k+K}, V\varphi_k)/S$[b] (ry) | $(\varphi_{k+K}, (V_{op}+V_R)\varphi_k)/S$[c] (ry) |
|---|---|---|
| [002] | −0.1950 | +0.047 |
| [100] | −0.1855 | +0.057 |
| [101] | −0.1675 | +0.081 |

[a] See reference 19, for notation.
[b] $V$ is the net ionic potential.
[c] $(\varphi_{k+K}, (V_{op}+V_R)\varphi_k)$ is the final matrix element.

[14] The author is indebted to D. S. Story for performing this portion of the calculation.
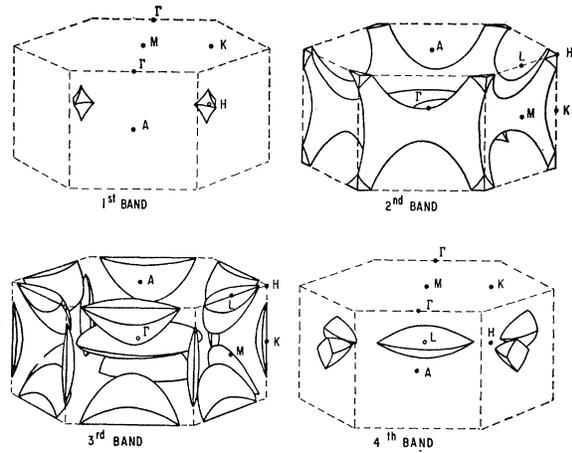[15] W. A. Harrison, Phys. Rev. 118, 1190 (1960).



FIG. 2. The one-OPW or nearly-free-electron Fermi surface for a divalent, hexagonal-close-packed metal of ideal $c/a$ ratio. Spin-orbit splittings are included with their consequent reduction of the double zone.

Finally, the band energy at various points of symmetry was calculated for the unscreened treatment, case (i), and listed in Table III as $E_{theo}$. The order of the secular equation used was for each symmetry point equal to the number of bands included in the table (with the exception of the point $\Gamma$, where a $2\times2$ determinent was solved).

## V. FERMI SURFACE AND EXPERIMENTAL BAND STRUCTURE

The Fermi surface for a divalent, hexagonal-close-packed metal in the one-OPW approximation[15,16] is given in Fig. 2. In no case in the preceding calculation did we find a matrix element which appreciably exceeded one-tenth of the Fermi energy, so we may expect this one-OPW approximation to be qualitatively correct when corrected for the modified $c/a$ ratio. In zinc the

TABLE III. Band energy at symmetry points. ($3d$-band: 0.122; Fermi energy: 0.708 ry.)

| Point and symmetry | $E_{theo}$ (ry) | $E_{exp}$ (ry) | Band |
|---|---|---|---|
| $\Gamma_1^+$ | 0 | 0 | 1 |
| $\Gamma_4^-$ | 0.449 | 0.411 | 2 |
| $\Gamma_3^+$ | 0.495 | 0.533 | 3 |
| $A_1$ | 0.118 | 0.118 | 1,2 |
| $M_2^-$ | 0.522 | 0.520 | 1 |
| $M_1^+$ | 0.526 | 0.528 | 2 |
| $L_1$ | 0.610 | 0.612 | 1,2 |
| $L_1$ | 0.674 | 0.671 | 3,4 |
| $K_5$ | 0.696 | 0.695 | 1,2 |
| $K_1$ | 0.703 | 0.706 | 3 |
| $H_2$ | 0.759 | 0.762 | 1,2 |
| $H_1$ | 0.821 | 0.824 | 3,4 |
| $H_3$ | 0.870 | 0.863 | 5,6 |

[16] M. H. Cohen and L. Falicov, Phys. Rev. Letters 5, 544 (1960); 7, 231 (1961).

$c/a$ ratio exceeds that of close packing by about 10%, which causes a shrinking of the Brillouin zone parallel to the $c$ axis by 10% from that shown.

There are several sets of de Haas-van Alphen periods which have been established experimentally. We will use the periods found by Joseph, Gordon, and Eck[17,18] in our analysis. The maximum periods (corresponding to minimum areas) of these and the corresponding segment of Fermi surface to which they belong according to current interpretation are:

(a) Vertical needles in the third band. The period[17] is $6.30 \times 10^{-5}$ gauss$^{-1}$, corresponding to an area of $0.426 \times 10^{-4}$ a.u. (units of wave number squared).

(b) Diagonal arms in the second band. The period[17,18] for these is $2.24 \times 10^{-7}$ gauss$^{-1}$, corresponding to an area of 0.0120 a.u. There are difficulties in the interpertation of these which will be discussed in Sec. VI of this paper.

(c) Horizontal arms in the second band. The period[17] is $2.23 \times 10^{-6}$ gauss$^{-1}$, corresponding to an area of 0.00120 a.u.

(d) The intersection in the second band with the hexagonal face of the second zone and the horizontal section of the bits in the first band.[17,18] These two sections of the surface are split off from each other by spin-orbit coupling[16] and the two distinct sections are seen. The average of the two periods[18] found is $1.59 \times 10^{-7}$ gauss$^{-1}$, corresponding to an area of 0.0169 a.u. The two areas observed are 3% above and below

this value. The splitting corresponds to a gap of a few thousandths of a rydberg in agreement with the estimate of Cohen and Falicov.[16] We will proceed by neglecting the spin-orbit coupling except in zero order as it modifies the connectivity of the surface. Thus, we will compute the average area only.

(e) The fifth set, which Joseph et al.[17] denote by $\delta$, they assign to an orbit which loops through the second-band rim and encloses the intersection of two diagonal arms and the rim. They find a period of $4.38 \times 10^{-8}$ gauss$^{-1}$, corresponding to an area of 0.061 a.u. with a field along the bisector of the lattice wave numbers [100] and [001].[19]

We cannot deduce the appropriate matrix elements from the known sections of the Fermi surface alone because of uncertainty of the sign of the matrix elements. However, we can assert values for the matrix elements and adjust them until the correct surface is obtained. A comparison of the observed periods to those of the nearly-free-electron approximation[15] and examination of which matrix elements affect each quickly indicates that the magnitude of the matrix element associated with the lattice wave number [100] is small in comparison with the other two. This was the case also with our unscreened calculations, so we start with these. All we need extract from these calculations is the assignment of signs to the matrix elements; we may then determine the matrix elements uniquely.

We start with the segment $a$, which depends sensitively only upon the matrix element [100]. We proceed to $b$ which depends both on [100] and [101], and then to $c$ which depends upon [101] and [002]. Finally, we estimate segments $d$ and $e$ as a check.

The procedure for making these determinations may be described as follows: We should write down a Hamiltonian matrix using a free-electron kinetic energy and matrix elements connecting all states with wave
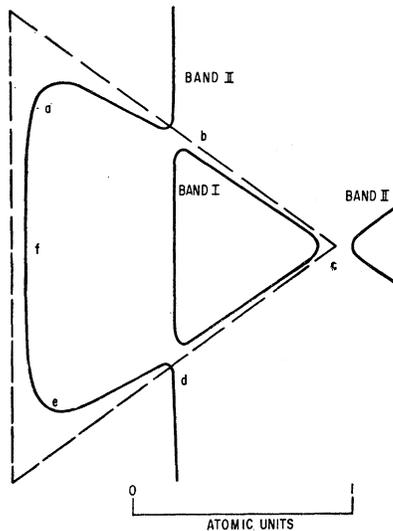


FIG. 3. Calculated minimum cross section of the diagonal arms using the experimental band structure. It is assumed that the orbit observed is $abcdef$, which requires magnetic breakdown at the points $b$ and $d$ but not at $c$; the orbit lies partly in band I and partly in band II. The dashed line represents the one-OPW (or free-electron) orbit.

TABLE IV. Matrix elements from experiment.

| Lattice wave number[a] | $(\varphi_{k+K}, (V_{op}+V_R)\varphi_k)/S$[b] (ry) | $S$ | |
|---|---|---|---|
| | | Mag. | Phase |
| [002] | −0.0612 | 1 | 0° |
| [100] | −0.0078 | 1/2 | −60° |
| [101] | +0.0337 | $\sqrt{3}/2$ | +30° |

[a] See reference 19 for notation.
[b] $(\varphi_{k+K}, (V_{op}+V_R)\varphi_k)$ is the final matrix element.

[17] A. S. Joseph and W. L. Gordon, Phys. Rev. 126, 489 (1962), preceding paper.
[18] A. S. Joseph, W. L. Gordon, J. R. Reitz, and T. G. Eck, Phys. Rev. Letters 7, 334 (1961).

[19] It will be convenient in discussing the band structure to specify all directions in wave-number space. A direction $[\alpha\beta\gamma]$ may be written as a linear combination of three lattice wave numbers, $\alpha K_1 + \beta K_2 + \gamma K_3$, where $K_1$ and $K_2$ are primitive lattice wave numbers perpendicular to the $c$ axis, which make an angle of 60° with each other, and $K_3$ is the primitive lattice wave number of the hexagonal lattice parallel to the $c$ axis. A direction $[\alpha\beta\gamma]$ in wave-number space is parallel to a direction $[2\alpha+\beta, 2\beta+\alpha, -3\alpha-3\beta, \frac{1}{2}\sqrt{3}(a/c)^2\gamma]$ in real space (using the four-index crystallographic notation).

number differing by a lattice wave number, and then solve for the eigenvalues as a function of wave number. We assume, however, that the main effect of these corrections leaves the Fermi surface nearly spherical except near the zone faces where particular matrix elements become important (the few-OPW approximation); we will, then, treat only those few matrix elements which are most important in a particular region.

A particular matrix element will do two things: First, it will distort the Fermi surface near the zone faces and second, it will shift the Fermi energy. We should, in principle, calculate the shift for each matrix element and then determine the Fermi surface at the new Fermi energy. These corrections, however, are small and we have not made them; the shift in Fermi energy due to the largest matrix element may readily be estimated by perturbation theory using the matrix element we calculate. It is 0.002 ry, which is unimportant for our purposes.

For the three segments of surface, $a$, $b$, and $c$, the problem reduces to the solution of a set of $3 \times 3$ matrices. These are set up and solved by techniques described earlier.[20] It was found convenient to use rectilinear co-

[20] Reference 3, Appendix I.

ordinates rather than polar coordinates and again the problem reduced to solving quadratic equations. For these small segments it was found convenient and quite accurate to take only the term in the kinetic energy which is linear in the wave number as measured from the center of the segment. In this approximation, the free-electron surfaces become triangular for segments $a$, $b$, $c$, and $d$.

By adjusting the matrix elements, the experimental areas were fit, and the resulting matrix elements are listed in Table IV. The agreement with the values from both band calculations is quite good. In particular, the largest correction to the values calculated without screening is less than 0.04 ry. These corrections should be compared to the terms in the matrix element before cancellation which were a few tenths of a rydberg.

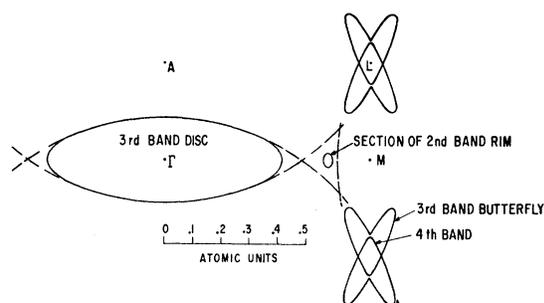Three interesting sections of the Fermi surface calculated from the experimental band structure are shown



FIG. 5. Sections of the Fermi surface in a plane perpendicular to a [100] direction and through $\Gamma$, calculated from the experimental band structure. Sections of surface which cross on the line $AH$ are split to left and right by spin-orbit coupling. Sections of surface which appear to cross on the line $KH$ correspond to a line of contact along $KH$ between the first and second bands. Above and below the section shown, this crossing is split up and down.

in Figs. 3 through 5. The interpretation of (b) in Sec. V is questionable, as seen in Fig. 3, and a check of the values obtained is necessary. This interpretation of Sec. V (b) will be discussed in Sec. VI on magnetic breakdown. Segment $d$ (which depends on the matrix elements [100] and [101]) and segment $e$ (which depends on the matrix elements [101] and [002]) were calculated from the matrix elements of Table IV. The area of the segment $d$ obtained was 0.0162, to be compared with the experimental average of 0.0169 a.u. The tiny discrepancy is certainly no greater than the errors arising from approximations in the graphical determination of the area. The area which Joseph et al. have associated with the periods $e$ was found to be 0.057 a.u., to be compared with the measured area of 0.061 a.u. Again the agreement is satisfactory and supports both our values from Table IV and the interpretation of the periods.

Finally, we calculated the energy values at various symmetry points using matrix elements as found by



FIG. 4. Sections of the Fermi surface in a plane perpendicular to a [110] direction and through $\Gamma$, calculated from the experimental band structure. Dashed lines represent one-OPW (or free-electron) Fermi surface. Sections of surface which cross are split from left to right by spin-orbit coupling.
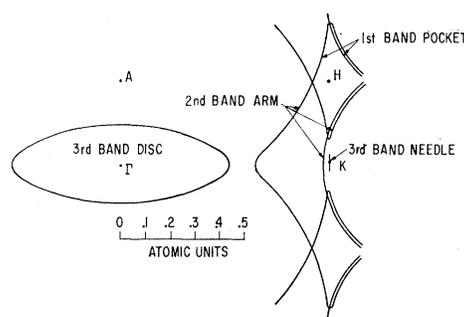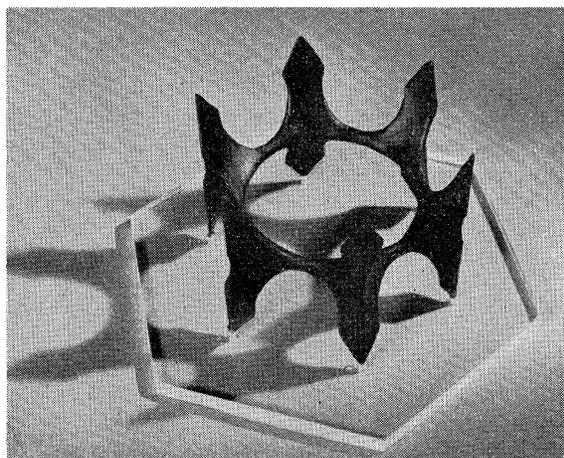


FIG. 6. A model of the Fermi surface in bands I and II, based on the experimental band structure. Spin-orbit coupling is omitted.

adjusting the Fermi surface; these are listed in Table III. Some error is introduced here by utilizing matrix elements evaluated on portions of the Brillouin zone face different from those appropriate to the symmetry point. In addition, there is some error associated with including only the effects of a few plane waves for each point. We expect the errors not to exceed a few hundredths of a rydberg.

## VI. MAGNETIC BREAKDOWN

Electrons may jump between bands when an applied magnetic field is sufficiently large.[18] It was necessary to assume that such jumping occurs in the interpretation of the periods which are associated with the diagonal arms in the second band (segment $b$). The symmetry of the variation of the period with orientation, the magnitude of the maximum period, and the rate of variation with rotation all support our interpretation of these periods and appear to rule out any other possibilities. On the other hand, detailed consideration of the band structure indicates that orbits around this section exist only if the electrons jump between bands at $b$ and $d$ but not at $c$ in Fig. 3. This might seem a little unlikely and should be investigated further.

We will do this by first making an intuitive extension of the theory into the intermediate field range, starting from the high-field limit. We consider a free electron executing an orbit in a magnetic field $H$ with frequency $\omega_c^0 = eH/mc$. We now introduce a Fourier component of the lattice potential with coefficient $V_K$ and calculate the probability of an electron being scattered out of the state $\mathbf{k}(t)$ into the state $\mathbf{k}(t) + \mathbf{K}$ by time-dependent perturbation theory. This involves a time integration over each crossing of a Bragg plane which the electron makes. The result for each crossing is

$$P_{\mathbf{k} \to \mathbf{k}+\mathbf{K}} = [(2\pi/\hbar)|V_K|^2]/(dE_{\mathbf{k}+\mathbf{K}}/dt) = 2\pi/\omega_c^0\tau^0,$$

where

$$\frac{1}{\tau^0} = \frac{|V_K|^2}{2\hbar E_F} \frac{k_F^2 H}{\mathbf{K} \cdot (\mathbf{k} \times \mathbf{H})}.$$

This is presumably the procedure used by Joseph et al.[17] The result appears to be equivalent to that of Blount[21] for the high-field limit. The calculation is valid only if the scattering probability per crossing is small. However, we note that (since there are two crossings of the plane) $2/\tau^0$ is the probability per unit time of an electron leaving the initial orbit. Further, $1/\tau^0$ is formally independent of the magnitude of the magnetic field so we regard it as a transition rate and extend it into the intermediate and low-field ranges. Then the probability of completing an orbit is still $\exp(-4\pi/\omega_c^0\tau^0)$, or the probability of making an individual jump is $\exp(-2\pi/\omega_c^0\tau^0)$. In the low-field limit this is the probability of jumping or tunneling between bands at each

[21] E. I. Blount (to be published), Eq. (III 14).

pass. Furthermore, this is simply the square of the amplitude factor given by Blount[21] for the low-field limit and is therefore essentially equivalent to his result. The probability of jumping between bands at each approach, given by

$$P = \exp\left\{ -\frac{\pi|V_K|^2}{\hbar\omega_c^0 E_F} \frac{k_F^2 H}{\mathbf{K} \cdot (\mathbf{k} \times \mathbf{H})} \right\}, \qquad (10)$$

where $\omega_c^0$ and $E_F$ are the free-electron values, is correct in the high- and in the low-field limits, so we may have some confidence in it in the intermediate range.

We now proceed to the case of interest in segment $b$. The matrix element in question is 0.0039 ry, according to our estimate, which leads to an exponent in Eq. (10) of 4.0 at 20 000 gauss, where we have taken the angular factor as unity. The probability of an electron jumping the two gaps and not the third in order to complete an orbit, then, is of the order of $\exp(-8.0)$, corresponding to an $\omega_c\tau$ of about $2\pi/8 \approx 0.8$, with $\omega_c$ being the cyclotron frequency for the orbit in question and $\tau$ entering the problem as it would for any scattering process. Taking the angular factor into account actually reduces $\omega_c\tau$ by a factor of about 2.

It seems unlikely that the strong observed oscillations are compatible with an $\omega_c\tau$ as small as this. However, $\omega_c\tau$ varies inversely with the square of $V_K^2$ in this range, and a smaller bandgap would lead to an enhanced $\omega_c\tau$. A maximum value of $\omega_c\tau = 3.3$ would be obtained with a bandgap about half of that which we determined. Such an error in the bandgap would not be surprising. It should be noted that, though the amplitude of the de Haas-van Alphen oscillation drops as $\exp(-2\pi/\omega_c\tau)$, it also contains a factor $(d^2A/dz^2)^{-\frac{1}{2}}$, where $dA/dz$ is the rate of change of sectional area of the arm with displacement parallel to its axis. This is larger by a factor of about thirty than the corresponding factor for the orbits $d$ which were also observed by Joseph et al.[18] We conclude that the association of the periods $b$ with the diagonal arms is tenable. Almost the same values of the matrix elements would be obtained if we disregarded these periods and evaluated the matrix elements from the periods $d$ or $e$.

In connection with magnetic breakdown, it is interesting to note that in considering the orbit seen at high fields, the presence of a possible Bragg reflection enters as a field-independent scattering time and is in this sense indistinguishable from impurity scattering. For an orbit seen at low fields, on the other hand, we calculate the $\omega_c\tau$ due to the possibility of tunneling between bands as

$$e^{-2\pi/\omega_c\tau} = (1 - e^{-2\pi/\omega_c^0\tau^0})^n$$

for a case with $n$ passes per orbit, corresponding to a scattering time which decreases as the field increases. It is also interesting to note that in the intermediate range both orbits may be simultaneously observable by, for example, the de Haas-van Alphen effect, but both would have reduced amplitude. In the case of

interest here, the low-field orbit does not have an extremal area and is therefore not observable.

## VII. SUMMARY

We have found a band structure for zinc both from a detailed band calculation and from experimental knowledge of the Fermi surface. These are consistent to within a few hundredths of a rydberg. There are errors in both determinations arising from using only a small number of plane waves in each case. The apparently accidental change of sign of the matrix elements in the interesting range of reciprocal lattice vectors seems to be real and will be important in further studies of the properties of zinc. The variation of the matrix elements with magnitude of lattice wave number in this range is similar for both treatments and is probably reasonably reliable. Also, the areas of the Fermi surface sections calculated are probably good to a few percent and the shapes comparably reliable.

On the other hand, since the energy values at symmetry points are not reliable beyond a few hundredths of a rydberg, the fact that the unscreened calculation and the dielectric-constant treatment are closer to experiment than the self-consistent treatment sheds no light on the relative merits of these treatments.

We may note, in particular, the errors involved in utilizing only a few plane waves and constant matrix elements. A fitting of this procedure to the results of Falicov's band calculations[6] on magnesium indicates that an individual matrix element, as determined from band values at different symmetry points, will differ by as much as a factor of 2. Furthermore, whereas we would always find the center of gravity of a collection of levels at a given symmetry point unchanged by the introduction of splittings, he finds shifts of the order of a hundredth of a rydberg. Such shifts could lead to large percentage errors in the experimental determination of small bandgaps, in particular for the small matrix element associated with the lattice wave number [100].

Finally, our formulas for magnetic breakdown are probably accurate in the intermediate range, though the extension into this range is in no sense rigorous.
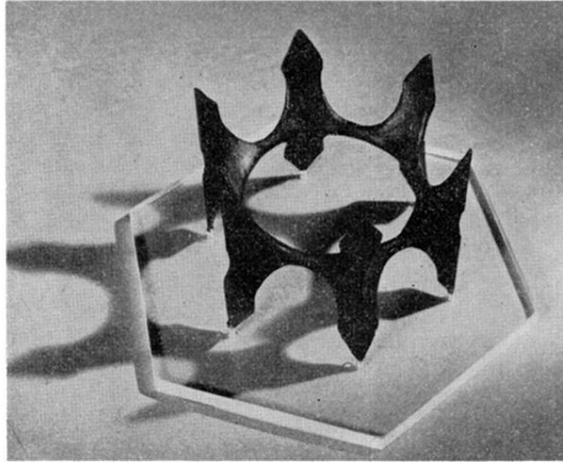
## ACKNOWLEDGMENTS

FIG. 6. A model of the Fermi surface in bands I and II, based on the experimental band structure. Spin-orbit coupling is omitted.